Propagating hydrodynamic modes in confined fluids

Fabien Porcheron* and Martin Schoen†

Stranski-Laboratorium für Physikalische und Theoretische Chemie, Sekretariat TC 7, Fakultät für Mathematik und Naturwissenschaften, Technische Universität Berlin, Straße des 17, Juni 124, D-10623 Berlin, Germany

(Received 12 March 2002; published 10 October 2002)

In molecular dynamics simulations in the microcanonical ensemble (MEMD) we calculate the intermediate scattering function $F(k_\parallel,t)$ for a ''simple'' fluid confined to nanoscopic slit pores with chemically homogeneous, planar substrate surfaces. Since system properties are translationally invariant in the x-y plane, we focus on the propagation of density modes *parallel* with the confining substrates by choosing a two-dimensional wave vector $|\boldsymbol{k}_\parallel|=k_\parallel=(k_x,k_y)$ for our analysis. Within the framework of classical hydrodynamics, we develop conservation laws for z-averaged fluxes of heat and momentum. Using in-plane versions of the macroscopic stress tensor and internal-energy current as constitutive equations we derive an expression for $F(k_\parallel,t)$ in the hydrodynamic limit depending on the thermal diffusivity D_T, the sound attenuation coefficient Γ, the in-plane adiabatic velocity of sound $v_\parallel$, and the ratio of heat capacities at constant transverse stress and volume γ. Through a fit of $F(k_\parallel,t)$ in the hydrodynamic limit and its associated memory function $M(k_\parallel,t)$ to MEMD data, reliable values for the set $\{D_T,\Gamma,v_\parallel,\gamma\}$ of material coefficients can be obtained. Variations in $\{D_T,\Gamma,v_\parallel,\gamma\}$ with s_z may be correlated with variations in the solvation pressure $-\tau_{zz}-P_b$ with s_z (τ_{zz} is the stress exerted by the fluid along the surface normal and P_b is the bulk pressure) and therefore linked to stratification of the confined fluid.

DOI: 10.1103/PhysRevE.66.041205 PACS number(s): 62.10.+s, 61.46.+w, 62.25.+g, 68.55.−a

I. INTRODUCTION

In a fluid (i.e., gas or liquid) equilibrium properties can be linked to the typical range of intermolecular correlations. If such a fluid is confined to spaces of nanoscopic dimension(s) by solid substrates, say, confinement (i.e., the separation s_z of the solid surfaces) adds a new relevant length scale and, as a consequence, fluid properties are altered markedly from those of a corresponding bulk fluid at the same temperature T and chemical potential μ. For example, in such a fluid, confinement-induced phase transitions may arise, which do not have a bulk counterpart [1]. Moreover, diffusion in confined monolayer films may be anomalous in that the time-dependence of the mean-square displacement in a direction parallel with the confining (planar) substrates may be fractal [2]. These and other unique features of confined fluids make them fascinating both from an experimental and from a theoretical perspective. However, to date, most of the work devoted to confined fluids is still concerned with equilibrium properties [3].

Comparatively few studies are therefore devoted to time-dependent phenomena in confined fluids [4] and most of these focus on diffusion [2,5,6], with particular emphasis on zeolites [7–9]. This interest is largely stimulated by important technical applications of these materials, such as molecular sieves [10] and catalysis [11]. Diffusion is also the rate-determining factor in the separation of binary gas mixtures in porous media [12–14].

Besides diffusion, viscous flow through microporous media has been the other focal point in recent years [15–19]. For example, Bitsanis *et al.* [15] developed the so-called local average density model (LADM) to describe fluid flow in directions parallel to the substrates. The LADM takes into account the inhomogeneity of the confined fluid along the substrate normal by introducing a viscosity that depends on the local average density at position z between the substrates. The local average density is obtained by averaging the local density over a spherical volume centered at z, with a diameter equal to the ''diameter'' σ of a (''simple'') fluid molecule. Travis *et al.* [16], and later on Travis and Gubbins [17], simulated Poiseuille flow in nanoscopic slits and observed velocity profiles in the direction normal to the substrate surfaces that cannot be accounted for by the constitutive equations of classical hydrodynamics. Based upon their observations Travis and Gubbins propose a modified constitutive equation for momentum flux by assuming that the shear viscosity depends on the position z relative to the substrates in the sense of a convolution integral involving also the local strain rate [see Eq. (5) in Ref. [17]].

To develop a better understanding of the viscous behavior of confined fluids is of interest in a number of contexts. Take as an example experiments employing the surface force apparatus (SFA), which permits one to measure the shear stress in response to an externally applied strain. A reproducible but still puzzling observation is that below a film thickness of about six molecular layers, a dramatic increase of the shear viscosity is reported, regardless of the molecular structure of the confined phase [20,21] that would normally signal solidification. However, the mismatch between the crystallographic structure of the confining (mica) substrates and solid structures that the confined phase would possibly form in the bulk renders solidification to be a rather unlikely cause of the experimentally observed increase in shear viscosity.

From a broader perspective, the viscous nature of a fluid is generally responsible for the damping of density modes, which can *in principle* be measured through the dynamic

*Electronic address: fabien@terra.chem.tu-berlin.de

†Electronic address: martin@terra.chem.tu-berlin.de

structure factor $S(\boldsymbol{k},\omega)$ by the scattering of light [22,23] or thermal neutrons [24]. On account of their difference in wavelength by about three orders of magnitude, light scattering provides information about slow ($\omega\to 0$), long-wavelength ($|\boldsymbol{k}|\to 0$) modes (i.e., hydrodynamic modes) whereas thermal neutrons permit insight into the dynamics of a fluid at the molecular scale due to their much shorter wavelengths corresponding roughly to σ as far as ''simple'' fluids are concerned.

Theoretically, $S(\boldsymbol{k},\omega)$ can be determined in molecular dynamics (MD) computer simulations. However, in MD, $S(\boldsymbol{k},\omega)$ is not directly accessible because the simulations are performed in the time (t) and not in the frequency (ω) domain. Hence, the intermediate scattering function $F(\boldsymbol{k},t)$, which is related to $S(\boldsymbol{k},\omega)$ through a Laplace transformation, is the more suitable quantity. At the microscopic level, $F(\boldsymbol{k},t)$ represents the time-dependent autocorrelation function of the Fourier components of the local density. Experimentally, $F(\boldsymbol{k},t)$ can be determined *directly* in neutron spin echo measurements [25,26].

In the hydrodynamic limit ($|\boldsymbol{k}|\equiv k\to 0,\ \omega\to 0$), $F(k,t)$ for bulk fluids can be expressed in terms of a set of material constants, such as the thermal diffusivity D_T and the kinematic viscosity b. However, if the hydrodynamic $F(k,t)$ is fitted to MD data over a k range typically accessible in MD without having to take recourse to anything but standard simulation techniques, these materials constants turn out to depend on k, thereby pointing to the fact that the hydrodynamic form of $F(k,t)$ is inadequate [27]. Since we are interested in properties like D_T and b for confined fluids, we develop here an approach based upon the memory function $M(k_\parallel,t)$ associated with $F(k_\parallel,t)$ where we focus exclusively on the density modes propagating in the x-y plane (i.e., *parallel* with the confining substrates) by choosing $\boldsymbol{k}_\parallel=(k_x,k_y)$. In developing the relevant hydrodynamic expressions we take advantage of the fact that across each x-y plane (located at different z), properties of the confined fluid are translationally invariant in our model.

The remainder of the paper is organized as follows. Section II A is devoted to a derivation of hydrodynamic conservation laws for slit pores. In Sec. II B, we are concerned with deriving a hydrodynamic equation for the evolution of density modes in slit pores. Starting from a microscopic definition of $F(k_\parallel,t)$ in Sec. III A, we derive its hydrodynamic counterpart in Sec. III B. Section III C is devoted to an introduction of the memory-function formalism used below in Sec. IV. Applications to bulk and confined fluids are then discussed in Secs. IV B and IV C, respectively. We finally summarize our findings in Sec. V.

II. HYDRODYNAMIC MODES IN CONFINED FLUIDS

A. Conservation laws for slit pores

Consider a time-dependent vector field

$$\boldsymbol{a}(\boldsymbol{r},t)=\sum_{i=1}^{N}\boldsymbol{a}_i(t)\,\delta[\boldsymbol{r}-\boldsymbol{r}_i(t)], \tag{2.1}$$

where $\boldsymbol{r}\in\mathbb{R}^3$, $\boldsymbol{r}_i(t)$ is the position of fluid molecule i at time t, and $\delta[\boldsymbol{r}-\boldsymbol{r}_i(t)]$ is the Dirac δ function. In Eq. (2.1), $\boldsymbol{a}_i(t)$ is a physical property of molecule, i and therefore $\boldsymbol{a}(\boldsymbol{r},t)$ is the local dynamical variable associated with it. For example, if $\boldsymbol{a}_i(t)$ were the momentum $\boldsymbol{p}_i(t)$ of molecule i, $\boldsymbol{a}(\boldsymbol{r},t)\equiv\boldsymbol{p}(\boldsymbol{r},t)$ would be the associated time-dependent local momentum density.

Following standard reasoning [28] it can be shown that $\boldsymbol{a}(\boldsymbol{r},t)$ satisfies the continuity equation

$$\partial_t\boldsymbol{a}(\boldsymbol{r},t)+\boldsymbol{\nabla}\cdot\mathbf{J}^{\boldsymbol{a}}(\boldsymbol{r},t)=\mathbf{0} \tag{2.2}$$

in the absence of sources and sinks, that is, $\boldsymbol{a}(\boldsymbol{r},t)$ is assumed to be conserved. In Eq. (2.2), $\partial_t\equiv\partial/\partial t$, and (Cartesian) components of the flux tensor $\mathbf{J}^{\boldsymbol{a}}(\boldsymbol{r},t)$ are given by

$$J^{\boldsymbol{a}}_{\alpha\beta}(\boldsymbol{r},t)=a_\alpha(\boldsymbol{r},t)v_\beta(\boldsymbol{r},t),\quad \alpha,\beta=x,y,z, \tag{2.3}$$

where $v_\beta(\boldsymbol{r},t)$ is the β component of the velocity field at $\boldsymbol{r}$ and t.

We now wish to apply these considerations to a slit pore with chemically homogeneous substrate surfaces located at $z=\pm s_z/2$. If s_z is of the order of the typical range of interactions between the fluid molecules, the pore fluid will be highly inhomogeneous, that is, molecules arrange their centers of mass such that the fluid consists of individual strata parallel with the confining substrate surfaces. This is reflected by the fluid's local density that is a damped oscillatory function of z [29]. Since we shall be concerned later only with a hydrodynamic analysis of *in-plane* fluxes, that is, fluxes *parallel* with the substrate planes, it is sensible to turn to ''reduced'' conservation laws. The latter are obtained by multiplying both sides of Eq. (2.2) by $s_z^{-1}dz$ and integrating the resulting expression over z which gives

$$\begin{aligned}\partial_t\overline{a}_\alpha(\boldsymbol{R},t)=&-\partial_x\overline{J^{\boldsymbol{a}}_{x\alpha}}(\boldsymbol{R},t)-\partial_y\overline{J^{\boldsymbol{a}}_{y\alpha}}(\boldsymbol{R},t)-J^{\boldsymbol{a}}_{z\alpha}(\boldsymbol{R},s_z/2,t)\\&+J^{\boldsymbol{a}}_{z\alpha}(\boldsymbol{R},-s_z/2,t),\quad \alpha=x,y,z,\end{aligned} \tag{2.4}$$

where $\boldsymbol{R}\in\mathbb{R}^2$ is a point in the x-y plane and

$$\overline{a}_\alpha(\boldsymbol{R},t)\equiv\frac{1}{s_z}\int_{-s_z/2}^{s_z/2}dz\,a_\alpha(\boldsymbol{R},z,t), \tag{2.5a}$$

$$\overline{J}_{\alpha\beta}(\boldsymbol{R},t)\equiv\frac{1}{s_z}\int_{-s_z/2}^{s_z/2}dz\,J_{\alpha\beta}(\boldsymbol{R},z,t). \tag{2.5b}$$

In Eq. (2.4)

$$J^{\boldsymbol{a}}_{\alpha\beta}(\boldsymbol{R},\pm s_z/2,t)=a_\alpha(\boldsymbol{R},\pm s_z/2,t)v_\beta(\boldsymbol{R},\pm s_z/2,t), \tag{2.6}$$

where

$$v_\beta(\boldsymbol{R},\pm s_z/2,t)=\sum_{i=1}^{N}v_{\beta i}(t)\,\delta[\boldsymbol{R}-\boldsymbol{R}_i(t)]\underbrace{\delta[\pm s_z/2-z_i(t)]}_{=0}=0 \tag{2.7}$$

expresses the fact that fluid molecules cannot reach the substrate surfaces located at $z=\pm s_z/2$ on account of diverging

fluid-substrate repulsion. From Eqs. (2.4) and (2.7), it is then clear that the last two terms on the right side of Eq. (2.4) vanish identically. It is now convenient to introduce the ''transverse'' tensor $[\mathbf{J}_{\parallel}^{a}(\boldsymbol{R},t)]_{\alpha\beta}\equiv\overline{J_{\alpha\beta}^{a}}(\boldsymbol{R},t)$ $(\alpha,\beta=x,y)$ and the ''normal'' vector $[\mathbf{J}_{\perp}^{a}(\boldsymbol{R},t)]_{\alpha}\equiv\overline{J_{\alpha z}^{a}}(\boldsymbol{R},t)$ $(\alpha=x,y)$ and recast Eq. (2.4) compactly as

$$\partial_t \boldsymbol{a}_{\parallel}(\boldsymbol{R},t)+\boldsymbol{\nabla}_{\parallel}\cdot\mathbf{J}_{\parallel}^{a}(\boldsymbol{R},t)=\mathbf{0}, \tag{2.8a}$$

$$\partial_t a_z(\boldsymbol{R},t)+\boldsymbol{\nabla}_{\parallel}\cdot\boldsymbol{J}_{\perp}^{a}(\boldsymbol{R},t)=0, \tag{2.8b}$$

where $\boldsymbol{a}_{\parallel}\equiv(a_x,a_y)$, $\boldsymbol{\nabla}_{\parallel}\equiv(\partial_x,\partial_y)$ $(\partial_\alpha\equiv\partial/\partial\alpha)$. In Eqs. (2.8), it should be understood that henceforth all (vector or scalar) fields depending only on $\boldsymbol{R}$ and t have been averaged over z in the above sense. We have therefore already dropped the overbar on $\overline{\boldsymbol{a}_{\parallel}}$ and $\overline{a_z}$ in Eqs. (2.8) to simplify the notation.

If, at the outset, we were concerned with a scalar rather than a vector field replacing in Eq. (2.1), $\boldsymbol{a}(\boldsymbol{r},t)$ and $\boldsymbol{a}_i(t)$ by their scalar analogs $a(\boldsymbol{r},t)$ and $a_i(t)$, similar considerations apply and the resulting z-averaged conservation law can be cast as

$$\partial_t a(\boldsymbol{R},t)+\boldsymbol{\nabla}_{\parallel}\cdot\boldsymbol{J}_{\parallel}^{a}(\boldsymbol{R},t)=0, \tag{2.9}$$

where the (z-averaged) vector $\boldsymbol{J}_{\parallel}^{a}\equiv(J_x^a,J_y^a)$ has only two components.

Moreover, since s_z is comparable to the range of intermolecular interactions, an analysis of propagating modes in terms of hydrodynamic equations makes only sense in the x-y plane. Thus, Eq. (2.8b) will not be employed henceforth. To reduce the notational burden even further, it then seems sensible to drop the subscript on the operator $\boldsymbol{\nabla}_{\parallel}$ as well as on the fluxes $\mathbf{J}_{\parallel}^{a}(\boldsymbol{R},t)$ and $\boldsymbol{J}_{\parallel}^{a}(\boldsymbol{R},t)$ from now on.

B. Density correlations

At this stage we introduce the constitutive equations

$$[\mathbf{J}^{p}(\boldsymbol{R},t)]_{\alpha\beta}=-\tau_{\parallel}(\boldsymbol{R},t)\,\delta_{\alpha\beta}-\eta[\partial_\beta v_\alpha(\boldsymbol{R},t)+\partial_\alpha v_\beta(\boldsymbol{R},t)]+\delta_{\alpha\beta}\left(\frac{2}{3}\eta-\zeta\right)\boldsymbol{\nabla}\cdot\boldsymbol{v}(\boldsymbol{R},t),\quad \alpha,\beta=x,y, \tag{2.10a}$$

$$\boldsymbol{J}^{u}(\boldsymbol{R},t)=h\boldsymbol{v}(\boldsymbol{R},t)-\lambda\boldsymbol{\nabla}T(\boldsymbol{R},t), \tag{2.10b}$$

for (z-averaged) in-plane momentum [see Eq. (2.10a)] and energy flux [see Eq. (2.10b)]. In Eqs. (2.10), $\tau_{\parallel}(\boldsymbol{R},t)$ is the lateral local stress, $\boldsymbol{v}(\boldsymbol{R},t)$ is the velocity field, η and ζ are, respectively, shear and bulk viscosities and $\delta_{\alpha\beta}$ is the Kronecker symbol. In Eq. (2.10b), $h=u-\tau_{\parallel}$ and u are, respectively, enthalpy and internal-energy density of a confined fluid in thermodynamic equilibrium, λ is the thermal conductivity, and $T(\boldsymbol{R},t)$ is the (z-averaged) local temperature. That is, we explicitly *assume* the same constitutive equations for the z-averaged lateral fluxes (i.e., fluxes parallel to the substrate surfaces) normally employed for homogeneous, isotropic bulk fluids [28,30]. This seems justified because the confined fluid is assumed macroscopic (i.e., of infinite extent) in the x and y directions. Moreover, since the substrate is chemically homogeneous and planar (see Sec. IV A), fluid properties are translationally invariant across the x-y planes. Consequently, if averaged over z, we are essentially dealing with a laterally *homogeneous* and *isotropic* fluid. Hence, the inadequacy of hydrodynamics to describe (Poiseuille) flow in narrow slits observed by Travis *et al.* [16] and later on by Travis and Gubbins [17] need not be of concern here. This is because this inadequacy was observed only if an expression similar to Eq. (2.10a) was employed to analyze the velocity profile along the surface *normal* where, in fact, the confined fluid is highly inhomogeneous. However, it is interesting to note that as a cure of the apparent deficiency of classical hydrodynamics, Travis and Gubbins propose to replace the constant shear viscosity in their constitutive equation by a local one, averaged over z [17]. This concept, which has not been fully tested to date, seems similar in spirit to the z-averaged conservation laws introduced in Sec. II A.

Inserting the constitutive equation (2.10a) into the conservation law for the momentum density $\boldsymbol{p}(\boldsymbol{R},t)$ [see Eq. (2.8a) for $\boldsymbol{a}\equiv\boldsymbol{p}$] and using

$$\boldsymbol{p}(\boldsymbol{R},t)=m\rho\boldsymbol{v}(\boldsymbol{R},t)=m\boldsymbol{J}^{\rho}(\boldsymbol{R},t), \tag{2.11}$$

where m is the mass of a fluid molecule, $\boldsymbol{J}^{\rho}(\boldsymbol{R},t)$ is the number-density flux, and $\rho=N/As_z$ is the mean number density at equilibrium, permits us to write

$$\partial_t\boldsymbol{J}^{\rho}(\boldsymbol{R},t)-\frac{1}{m}\boldsymbol{\nabla}\tau_{\parallel}(\boldsymbol{R},t)-\frac{\eta}{\rho m}\nabla^2\boldsymbol{J}^{\rho}(\boldsymbol{R},t)-\frac{\frac{1}{3}\eta+\zeta}{\rho m}\boldsymbol{\nabla}[\boldsymbol{\nabla}\cdot\boldsymbol{J}^{\rho}(\boldsymbol{R},t)]=\mathbf{0}, \tag{2.12}$$

which is the z-averaged, in-plane analog of the linearized three-dimensional Navier-Stokes equation [30]. Similarly, starting from the conservation law for the local (internal-) energy density $u(\boldsymbol{R},t)$ [$a\equiv u$, see Eq. (2.9)] and using the constitutive equation (2.10b) we have

$$\partial_t\left[u(\boldsymbol{R},t)-\frac{u-\tau_{\parallel}}{\rho}\rho(\boldsymbol{R},t)\right]-\lambda\nabla^2T(\boldsymbol{R},t)=\partial_t q(\boldsymbol{R},t)-\lambda\nabla^2T(\boldsymbol{R},t)=0, \tag{2.13}$$

where $q(\boldsymbol{R},t)$ is the local heat density following the line of arguments presented in Ref. [31]. To arrive at Eq. (2.13), we used Eqs. (2.11) and (2.9) for $a\equiv\rho$.

Perceiving now $\tau_{\parallel}(\boldsymbol{R},t)$ and $q(\boldsymbol{R},t)$ as functions of average density and temperature of the confined fluid, we expand both quantities in terms of deviations $\delta\rho(\boldsymbol{R},t)=\rho(\boldsymbol{R},t)-\rho$ and $\delta T(\boldsymbol{R},t)=T(\boldsymbol{R},t)-T$ of $\rho(\boldsymbol{R},t)$ and $T(\boldsymbol{R},t)$ from their equilibrium values ρ and T to first order and get

$$\delta\tau_{\parallel}(\boldsymbol{R},t)=\left(\frac{\partial\tau_{\parallel}}{\partial\rho}\right)_{N,T,s_z}\delta\rho(\boldsymbol{R},t)+\left(\frac{\partial\tau_{\parallel}}{\partial T}\right)_{N,A,s_z}\delta T(\boldsymbol{R},t), \tag{2.14a}$$

$$\delta q(\boldsymbol{R},t)=\frac{T}{\rho}\left(\frac{\partial\tau_{\parallel}}{\partial T}\right)_{N,A,s_z}\delta\rho(\boldsymbol{R},t)+\rho c_{As_z}\delta T(\boldsymbol{R},t). \tag{2.14b}$$

Here we notice that at fixed N and s_z, $As_z dq(A,T)=Td\mathcal{S}(A,T)$ ($\mathcal{S}$ is the entropy) through the second law of thermodynamics, define the isochoric heat capacity per molecule $c_{As_z}\equiv TN^{-1}(\partial\mathcal{S}/\partial T)_{N,A,s_z}$, and utilize the Maxwell relation [32]

$$-\left(\frac{\partial\mathcal{S}}{\partial A}\right)_{N,T,s_z}=s_z\left(\frac{\partial\tau_{\parallel}}{\partial T}\right)_{N,A,s_z}. \tag{2.15}$$

To proceed, we notice that in Eq. (2.12), $\tau_{\parallel}(\boldsymbol{R},t)$ can be replaced by $\delta\tau_{\parallel}(\boldsymbol{R},t)=\tau_{\parallel}(\boldsymbol{R},t)-\tau_{\parallel}$, since $\boldsymbol{\nabla}\tau_{\parallel}$ vanishes identically. Employing then Eq. (2.14a) we may replace $\boldsymbol{\nabla}\delta\tau_{\parallel}(\boldsymbol{R},t)$ in Eq. (2.12) to obtain

$$\begin{aligned}\partial_t\boldsymbol{J}^{\rho}(\boldsymbol{R},t)&-\frac{1}{m}\left(\frac{\partial\tau_{\parallel}}{\partial\rho}\right)_{N,T,s_z}\boldsymbol{\nabla}\delta\rho(\boldsymbol{R},t)\\&-\frac{1}{m}\left(\frac{\partial\tau_{\parallel}}{\partial T}\right)_{N,A,s_z}\boldsymbol{\nabla}\delta T(\boldsymbol{R},t)-\frac{\eta}{\rho m}\nabla^2\boldsymbol{J}^{\rho}(\boldsymbol{R},t)\\&-\frac{\frac{1}{3}\eta+\zeta}{\rho m}\boldsymbol{\nabla}[\boldsymbol{\nabla}\cdot\boldsymbol{J}^{\rho}(\boldsymbol{R},t)]=\mathbf{0}.\end{aligned} \tag{2.16}$$

By similar arguments we may substitute in Eq. (2.13), $\delta q(\boldsymbol{R},t)$ and $\delta T(\boldsymbol{R},t)$ for $q(\boldsymbol{R},t)$ and $T(\boldsymbol{R},t)$, respectively. Dividing both sides of the resulting expression by ρc_{As_z} we get

$$\left(\partial_t-\frac{\lambda}{\rho c_{As_z}}\nabla^2\right)\delta T(\boldsymbol{R},t)+\frac{T}{\rho^2 c_{As_z}}\left(\frac{\partial\tau_{\parallel}}{\partial T}\right)_{N,A,s_z}\partial_t\delta\rho(\boldsymbol{R},t)=0. \tag{2.17}$$

Moreover, we have from Eq. (2.9)

$$\partial_t\rho(\boldsymbol{R},t)+\boldsymbol{\nabla}\cdot\boldsymbol{J}^{\rho}(\boldsymbol{R},t)=\partial_t\delta\rho(\boldsymbol{R},t)+\boldsymbol{\nabla}\cdot\boldsymbol{J}^{\rho}(\boldsymbol{R},t)=0, \tag{2.18}$$

so that Eq. (2.17) can be written in final form as

$$\left(\partial_t-\frac{\lambda}{\rho c_{As_z}}\nabla^2\right)\delta T(\boldsymbol{R},t)-\frac{T}{\rho^2 c_{As_z}}\left(\frac{\partial\tau_{\parallel}}{\partial T}\right)_{N,A,s_z}\boldsymbol{\nabla}\cdot\boldsymbol{J}^{\rho}(\boldsymbol{R},t)=0. \tag{2.19}$$

To solve the resulting coupled partial differential equations in Eqs. (2.16) and (2.19), we introduce the two-dimensional Fourier-Laplace transformation through Ref. [31] [$\boldsymbol{k}_{\parallel}\equiv(k_x,k_y)$],

$$\boldsymbol{a}(\boldsymbol{k}_{\parallel},s)=\int_0^{\infty}dt\,\exp(-st)\int d\boldsymbol{R}\,\delta\boldsymbol{a}(\boldsymbol{R},t)\exp(-i\boldsymbol{k}_{\parallel}\cdot\boldsymbol{R}). \tag{2.20}$$

Applying it to Eqs. (2.16), (2.18), and (2.19), we obtain a set of coupled linear equations for the unknown quantities $\rho(\boldsymbol{k}_{\parallel},s)$, $T(\boldsymbol{k}_{\parallel},s)$, and $\boldsymbol{J}^{\rho}(\boldsymbol{k}_{\parallel},s)$ expressed conveniently as

$$\underbrace{\begin{pmatrix} s & 0 & ik_{\parallel}\\ 0 & s+ak_{\parallel}^2 & -\dfrac{ik_{\parallel}T}{\rho^2 c_{As_z}}\left(\dfrac{\partial\tau_{\parallel}}{\partial T}\right)_{\rho}\\ -\dfrac{ik_{\parallel}}{m}\left(\dfrac{\partial\tau_{\parallel}}{\partial\rho}\right)_{T} & -\dfrac{ik_{\parallel}}{m}\left(\dfrac{\partial\tau_{\parallel}}{\partial T}\right)_{\rho} & s+bk_{\parallel}^2\end{pmatrix}}_{\mathbf{H}(k_{\parallel},s)}\begin{pmatrix}\rho(\boldsymbol{k}_{\parallel},s)\\ T(\boldsymbol{k}_{\parallel},s)\\ J^{\rho}(\boldsymbol{k}_{\parallel},s)\end{pmatrix}=\begin{pmatrix}\rho(\boldsymbol{k}_{\parallel})\\ T(\boldsymbol{k}_{\parallel})\\ J^{\rho}_{\parallel}(\boldsymbol{k}_{\parallel})\end{pmatrix}, \tag{2.21}$$

where $k_{\parallel}=|\boldsymbol{k}_{\parallel}|$ and $J^{\rho}=|\boldsymbol{J}^{\rho}|$ because of the translational invariance of system properties in the x-y plane. In the hydrodynamic matrix $\mathbf{H}(k_{\parallel},s)$, $a\equiv\lambda/\rho c_{As_z}$, and $b\equiv(\frac{4}{3}\eta+\zeta)/\rho m$ is the lateral kinematic viscosity. In Eq. (2.21), we have again simplified the notation by dropping the argument $t=0$ of the vector elements on the right side. We note that $\mathbf{H}(k_{\parallel},s)$ is formally equivalent to that part of $\mathbf{H}_b(k,s)$ for bulk fluids describing the propagation of hydrodynamic modes in the direction *parallel* with $\boldsymbol{k}=(k_x,k_y,k_z)$. However, on account of averaging the conservation laws over z [see Eqs. (2.8a) and (2.9)], $\mathbf{H}(k_{\parallel},s)$ is a 3×3 rather than a 5×5 matrix such as $\mathbf{H}_b(k,s)$, where one is also dealing with modes propagating in a direction *perpendicular* to $\boldsymbol{k}$ [see, for example, Eq. (8.3.28) in Ref. [31]].

However, the modes parallel and perpendicular to $\boldsymbol{k}$ are uncoupled. Therefore, the analysis of Eq. (2.21) is identical to that of the submatrix of $\mathbf{H}_b(k,s)$ for modes parallel to $\boldsymbol{k}$. For example, Eq. (2.21) reveals that the desired solution $\rho(\boldsymbol{k}_{\parallel},s)$ depends in general on $\rho(\boldsymbol{k}_{\parallel})$, $T(\boldsymbol{k}_{\parallel})$, and $J^{\rho}(\boldsymbol{k}_{\parallel})$. However, as pointed out by Hansen and McDonald for the

bulk counterpart of Eq. (2.21), $\rho(\boldsymbol{k}_\parallel,s)$ cannot depend on $T(\boldsymbol{k}_\parallel)$ since the latter and $\rho(\boldsymbol{k}_\parallel)$ are uncorrelated [31]. Moreover, one may choose $\boldsymbol{k}_\parallel$ so that initially (i.e., for $t=0$), $\boldsymbol{k}_\parallel$ is perpendicular to the mass flux. Thus, when solving Eqs. (2.21) for $\rho(\boldsymbol{k}_\parallel,s)$, $J^\rho(\boldsymbol{k}_\parallel)$ may be set to zero without the loss of generality. Therefore, one has

$$\rho(\boldsymbol{k}_\parallel,s)=\frac{H^{11}(k_\parallel,s)}{\det H(k_\parallel,s)}\rho(\boldsymbol{k}_\parallel), \tag{2.22}$$

where

$$\det H(k_\parallel,s)=s(s+ak_\parallel^2)(s+bk_\parallel^2)+sv_\parallel^2k_\parallel^2+\frac{a}{\gamma}v_\parallel^2k_\parallel^4, \tag{2.23}$$

and the algebraic complement is given by

$$H^{11}(k_\parallel,s)=(s+ak_\parallel^2)(s+bk_\parallel^2)+\frac{\gamma-1}{\gamma}v_\parallel^2k_\parallel^2. \tag{2.24}$$

To arrive at Eqs. (2.23) and (2.24), the definitions

$$\left(\frac{\partial\tau_\parallel}{\partial\rho}\right)_{N,T,s_z}=-\frac{mv_\parallel^2}{\gamma}, \tag{2.25a}$$

$$\left(\frac{\partial\tau_\parallel}{\partial T}\right)_{N,A,s_z}=\frac{v_\parallel^2m\rho^2}{T\gamma}(c_{\tau_\parallel}-c_{As_z}) \tag{2.25b}$$

have also been employed. In Eqs. (2.25), $v_\parallel$ is the adiabatic, in-plane velocity of sound defined analogously to its bulk counterpart [30], and $\gamma\equiv c_{\tau_\parallel}/c_{As_z}$, where $c_{\tau_\parallel}$ and c_{As_z} are, respectively, the heat capacities (per particle) at constant transverse stress and volume [32].

III. THE INTERMEDIATE SCATTERING FUNCTION

A. Microscopic definition

At a microscopic level, the temporal evolution of the local density is related to the so-called van Hove function defined as [31,33]

$$G(\boldsymbol{r},\boldsymbol{r}',t)=\frac{1}{N}\left\langle\sum_{l=1}^{N}\sum_{m=1}^{N}\delta[\boldsymbol{r}'+\boldsymbol{r}-\boldsymbol{r}_m(t)]\delta(\boldsymbol{r}'-\boldsymbol{r}_l)\right\rangle, \tag{3.1}$$

whose physical significance is that of the probability (density) of finding molecule m at a point $\boldsymbol{r}'+\boldsymbol{r}$ and time t, given that molecule l was located at point $\boldsymbol{r}'$ at $t=0$. Note that $G(\boldsymbol{r},\boldsymbol{r}',t)$ accounts for self-correlations ($m=l$) and cross correlations ($m\neq l$) (usually referred to as "distinct"). In Eq. (3.1) and below, we omit the argument $t=0$ of $\boldsymbol{r}_l$ and related quantities to ease the notational burden. The angular brackets in Eq. (3.1) denote an ensemble average. Considering the symmetry of our system we rewrite Eq. (3.1) as

$$G(\boldsymbol{R},\boldsymbol{R}',z,z',t)=\frac{1}{N}\left\langle\sum_{l=1}^{N}\sum_{m=1}^{N}\delta[\boldsymbol{R}'+\boldsymbol{R}-\boldsymbol{R}_m(t)]\times\delta(\boldsymbol{R}'-\boldsymbol{R}_l)\delta[z'+z-z_m(t)]\times\delta(z'-z_l)\right\rangle. \tag{3.2}$$

At equilibrium, system properties are translationally invariant in the x and y directions, so that we may integrate $G(\boldsymbol{R},\boldsymbol{R}',z,z',t)$ over the origin $\boldsymbol{R}'$ to get

$$G(\boldsymbol{R},z,z',t)=\frac{1}{N}\left\langle\sum_{l=1}^{N}\sum_{m=1}^{N}\delta[\boldsymbol{R}+\boldsymbol{R}_l-\boldsymbol{R}_m(t)]\times\delta[z''-z_m(t)]\delta(z'-z_l)\right\rangle, \tag{3.3}$$

where $z''\equiv z+z'$ has also been introduced. For the subsequent analysis in Sec. III B, it is convenient to *define* a "reduced" van Hove function that we obtain by integrating $G(\boldsymbol{R},z,z',t)$ in Eq. (3.3) over z' and z''. Two-dimensional Fourier transformation of the resulting $G(\boldsymbol{R},t)$ then gives the intermediate scattering function of a classical system

$$\tilde{F}(\boldsymbol{k}_\parallel,t)=\frac{1}{N}\left\langle\sum_{l=1}^{N}\sum_{m=1}^{N}\int\exp(-i\boldsymbol{k}_\parallel\cdot\boldsymbol{R})\times\delta[\boldsymbol{R}+\boldsymbol{R}_l-\boldsymbol{R}_m(t)]d\boldsymbol{R}\right\rangle, \tag{3.4}$$

where $\boldsymbol{k}_\parallel\equiv(k_x,k_y)$ is a two-dimensional vector in reciprocal space as before [see Eq. (2.20)]. Thus, $\tilde{F}(\boldsymbol{k}_\parallel,t)$ accounts for lateral correlations between molecules regardless of their separation along the z axis. By making use of an elementary property of the δ function, the last expression may be converted into

$$\tilde{F}(\boldsymbol{k}_\parallel,t)=\frac{1}{N}\left\langle\sum_{l=1}^{N}\sum_{m=1}^{N}\int\int\exp(-i\boldsymbol{k}_\parallel\cdot\boldsymbol{R})\times\delta[\boldsymbol{R}+\boldsymbol{R}_l-\boldsymbol{R}']\delta[\boldsymbol{R}'-\boldsymbol{R}_m(t)]d\boldsymbol{R}d\boldsymbol{R}'\right\rangle. \tag{3.5}$$

Transforming $\boldsymbol{R}\rightarrow\boldsymbol{R}''=\boldsymbol{R}-\boldsymbol{R}'$ in Eq. (3.5), we arrive at

$$\begin{aligned}\tilde{F}(k_\parallel,t)&=\frac{1}{N}\left\langle\sum_{l=1}^{N}\int\exp(-i\boldsymbol{k}_\parallel\cdot\boldsymbol{R}'')\delta[\boldsymbol{R}''+\boldsymbol{R}_l]d\boldsymbol{R}''\times\sum_{m=1}^{N}\int\exp(i\boldsymbol{k}_\parallel\cdot\boldsymbol{R}')\delta[\boldsymbol{R}'-\boldsymbol{R}_m(t)]d\boldsymbol{R}'\right\rangle\\&=\frac{1}{N}\langle\rho(-\boldsymbol{k}_\parallel)\rho(\boldsymbol{k}_\parallel,t)\rangle,\end{aligned} \tag{3.6}$$

where

$$\rho(\boldsymbol{k}_\parallel,t)=\sum_{m=1}^{N}\int \exp(-i\boldsymbol{k}_\parallel\cdot\boldsymbol{R}')\,\delta[\boldsymbol{R}'-\boldsymbol{R}_m(t)]\,d\boldsymbol{R}'$$

$$=\sum_{m=1}^{N}\exp[-i\boldsymbol{k}_\parallel\cdot\boldsymbol{R}_m(t)]. \tag{3.7}$$

In Eq. (3.6), we again exploit the fact that system properties are translationally invariant in the x-y plane and therefore $\tilde{F}(k_\parallel,t)$ must depend only on the *magnitude* and not on the *direction* of $\boldsymbol{k}_\parallel$. For $t=0$, $\langle\rho(-\boldsymbol{k}_\parallel)\rho(\boldsymbol{k}_\parallel)\rangle=NS(k_\parallel)$, where $S(k_\parallel)$ is the static structure factor. Thus, we introduce the *normalized* intermediate scattering function

$$F(k_\parallel,t)=\frac{\tilde{F}(k_\parallel,t)}{S(k_\parallel)}=\frac{\langle\rho(-\boldsymbol{k}_\parallel)\rho(\boldsymbol{k}_\parallel,t)\rangle}{\langle\rho(-\boldsymbol{k}_\parallel)\rho(\boldsymbol{k}_\parallel)\rangle}, \tag{3.8}$$

whose Laplace transform is given by

$$F(k_\parallel,s)=\frac{\langle\rho(-\boldsymbol{k}_\parallel)\rho(\boldsymbol{k}_\parallel,s)\rangle}{\langle\rho(-\boldsymbol{k}_\parallel)\rho(\boldsymbol{k}_\parallel)\rangle}. \tag{3.9}$$

B. The hydrodynamic limit

Inserting now Eq. (2.22), into Eq. (3.9) we obtain

$$F(k_\parallel,s)=\frac{(s+ak_\parallel^2)(s+bk_\parallel^2)+(\gamma-1)v_\parallel^2k_\parallel^2/\gamma}{s(s+ak_\parallel^2)(s+bk_\parallel^2)+sv_\parallel^2k_\parallel^2+(a/\gamma)v_\parallel^2k_\parallel^4}. \tag{3.10}$$

To transform F to the time domain, we follow the procedure described by Mountain [34] and later by McIntyre and Sengers [35] and split the far right side of Eq. (3.10) into partial fractions. This requires knowledge of the roots of the denominator. The roots may be approximated as follows. First, we transform variables in the denominator according to $s\rightarrow z=s/v_\parallel k_\parallel$ and introduce $x=ak_\parallel^2/v_\parallel k_\parallel$ and $y=bk_\parallel^2/v_\parallel k_\parallel$. Assuming both x and y to be sufficiently small [35], we expand the solution of the transformed cubic polynomial

$$z^3+z^2(x+y)+z(1+xy)+\frac{x}{\gamma}=0 \tag{3.11}$$

into a power series $z=a_0+a_1x+a_2y+\cdots$ cut off after the linear terms. Inserting this into Eq. (3.11) permits one to determine the unknown coefficients a_0, a_1, and a_2 by requiring terms of equal power in x and y to vanish separately. Thus, after transforming back to the original variables, zeros of the denominator are approximately given by [34,35,28]

$$s_0=-D_Tk_\parallel^2+O(k_\parallel^3), \tag{3.12a}$$

$$s_+=iv_\parallel k_\parallel-\Gamma k_\parallel^2+O(k_\parallel^3), \tag{3.12b}$$

$$s_-=-iv_\parallel k_\parallel-\Gamma k_\parallel^2+O(k_\parallel^3), \tag{3.12c}$$

where $D_T\equiv a/\gamma$ is the thermal diffusivity and $\Gamma=\frac{1}{2}[D_T(\gamma-1)+b]$ is the sound attenuation coefficient. Equations (3.12) agree formally with the results presented by McIntyre and Sengers [35] for the bulk. With Eqs. (3.12) we obtain from Eq. (3.10)

$$F(k_\parallel,s)=\frac{\gamma-1}{\gamma}\frac{1}{s+D_Tk_\parallel^2}+\frac{1}{2\gamma}\left\{\frac{1}{s-iv_\parallel k_\parallel+\Gamma k_\parallel^2}[1-id(k_\parallel)]\right.$$

$$\left.+\frac{1}{s+iv_\parallel k_\parallel+\Gamma k_\parallel^2}[1+id(k_\parallel)]\right\}, \tag{3.13}$$

where $d(k_\parallel)=[\Gamma k_\parallel^2+(\gamma-1)D_Tk_\parallel^2]/v_\parallel k_\parallel$ [27]. Equation (3.13) may then be transformed back into the time domain yielding

$$F(k_\parallel,t)=\frac{\gamma-1}{\gamma}\exp(-D_Tk_\parallel^2t)+\frac{1}{\gamma}\exp(-\Gamma k_\parallel^2t)$$

$$\times[\cos(v_\parallel k_\parallel t)+d(k_\parallel)\sin(v_\parallel k_\parallel t)]. \tag{3.14}$$

Equation (3.14) for the in-plane intermediate scattering function in the hydrodynamic limit is formally equivalent to its bulk counterpart first presented by Berne [36] and later on by Schoen *et al.* [27]. It differs, however, from the corresponding expression of McIntyre and Sengers [35] in the additional sin term (see also discussion in Ref. [27]).

C. Memory function

In principle, Eq. (3.14) may be employed to interpret results obtained in MD simulations [27]. However, one has to be aware of several crucial approximations made during its derivation. First, Eq. (3.14) applies only to situations where $v_\parallel$ is sufficiently large. It is therefore not applicable as one approaches a spinodal or a critical point, since there $\kappa_\parallel=-\rho^{-1}(\partial\rho/\partial\tau_\parallel)_{N,T,s_z}\propto v_\parallel^{-1}\rightarrow\infty$ (i.e., $v_\parallel\rightarrow0$) [see Eq. (2.25a)]. However, we have explicitly assumed in Sec. III B that $x,y\propto v_\parallel^{-1}\ll1$ [see Eqs. (3.11) and (3.12)]. Moreover, the *form* of the expression in Eq. (3.14) is only correct to order $O(k_\parallel^2)$. Hence, if $k_\parallel$ is not small enough, one expects Eq. (3.14) to hold only if all material constants (i.e., the set $\{D_T,\Gamma,\gamma,v_\parallel\}$) become $k_\parallel$ dependent. An extrapolation to the infinite-system limit $k_\parallel\rightarrow0$ may then become prohibitively difficult and is not free of arbitrariness (see, for example, Fig. 12 of Ref. [27]).

A determination of D_T, Γ, γ, and $v_\parallel$ not plagued by this deficiency is, however, possible by considering the memory function $M(k_\parallel,t)$ associated with $F(k_\parallel,t)$. Since $F(k_\parallel,t)$ is a time-dependent autocorrelation function [see Eq. (3.6)], it satisfies the Volterra integrodifferential equation

$$-\frac{dF(k_\parallel,t)}{dt}=\int_0^t dt'\,M(k_\parallel,t)F(k_\parallel,t-t'),\quad\forall\ k_\parallel \tag{3.15}$$

which, after Laplace transformation, may be solved for the memory kernel

$$M(k_\parallel,s)=\frac{1}{F(k_\parallel,s)}-s$$
$$=\frac{sv_\parallel^2k_\parallel^2/\gamma+(a/\gamma)v_\parallel^2k_\parallel^4}{(s+ak_\parallel^2)(s+bk_\parallel^2)+(\gamma-1)v_\parallel^2k_\parallel^2/\gamma}, \tag{3.16}$$

where we also used Eq. (3.10). Equation (3.16) can be transformed back to the time domain utilizing the zeros,

$$s_\pm=-\left(\Gamma k_\parallel^2+\frac{D_T}{2}k_\parallel^2\right)$$
$$\pm i\sqrt{\frac{v_\parallel^2k_\parallel^2}{\gamma}(\gamma-1)-\frac{1}{4}[D_Tk_\parallel^2(2\gamma-1)-2\Gamma k_\parallel^2]^2}$$
$$=-x'\pm ix'', \tag{3.17}$$

of the polynomial in the denominator. We may then rewrite Eq. (3.16) as

$$M(k_\parallel,s)=\frac{sv_\parallel^2k_\parallel^2/\gamma}{(s+x'+ix'')(s+x'-ix'')}$$
$$+\frac{D_Tv_\parallel^2k_\parallel^4}{(s+x'+ix'')(s+x'-ix'')}$$
$$=\frac{v_\parallel^2k_\parallel^2}{\gamma}[M'(k_\parallel,s)+D_T\gamma k_\parallel^2M''(k_\parallel,s)]$$
$$=M_0(k_\parallel)[M'(k_\parallel,s)+D_T\gamma k_\parallel^2M''(k_\parallel,s)]. \tag{3.18}$$

From $M'(k_\parallel,s)$ and $M''(k_\parallel,s)$, we obtain

$$M'(k_\parallel,t)=\frac{1}{2ix''}\{(x'+ix'')\exp[-(x'+ix'')t]$$
$$-(x'-ix'')\exp[-(x'-ix'')t]\}, \tag{3.19a}$$

$$M''(k_\parallel,t)=-\frac{1}{2ix''}\{\exp[-(x'+ix'')t]$$
$$-\exp[-(x'-ix'')t]\}, \tag{3.19b}$$

so that from Eqs. (3.18) and (3.19) one has

$$M(k_\parallel,t)=M_0(k_\parallel)\exp(-x't)[\cosh(ix''t)-iy''\sinh(ix''t)] \tag{3.20}$$

for the memory function in the hydrodynamic regime, where

$$y''\equiv\sqrt{\frac{M_0(\gamma-1)}{x''^2}-1}. \tag{3.21}$$

In the context of this work we shall assume that the inequality

$$M_0(k_\parallel)>\frac{(D_Tk_\parallel^2\gamma-x')^2}{\gamma-1} \tag{3.22}$$

is satisfied so that $x''\in\mathbb{R}$ [see Eqs. (3.17), (3.18)]. We may then rewrite Eq. (3.20) as

$$M(k_\parallel,t)=M_0(k_\parallel)\exp(-x't)[\cos(x''t)+y''\sin(x''t)], \tag{3.23}$$

since for $x''\in\mathbb{R}$, $\cosh(ix''t)=\cos(x''t)$ and $\sinh(ix''t)=i\sin(x''t)$.

IV. RESULTS

A. Technical details

We consider a fluid composed of N spherically symmetric molecules without internal degrees of freedom (i.e., ''simple'' molecules) squeezed between plane parallel solid substrates separated by s_z. Solid atoms forming the substrates interact with the fluid molecules *via* the pairwise additive potential

$$\varphi^{[k]}(z)=2\pi\epsilon\rho_s\sigma^2\left[\frac{2}{5}\left(\frac{\sigma}{z\pm s_z/2}\right)^{10}-\left(\frac{\sigma}{z\pm s_z/2}\right)^4\right], \tag{4.1}$$

where $+\leftrightarrow k=1$ and $-\leftrightarrow k=2$ refer to lower and upper substrates, respectively. In Eq. (4.1), the areal density of the solid substrate is set to $\rho_s\sigma^2=1$.

The fluid-fluid interaction is described by a so-called shifted-force potential defined by

$$u_{sf}(r)=\begin{cases}u_{\mathrm{LJ}}(r)-u_{\mathrm{LJ}}(r_c)+u'_{\mathrm{LJ}}(r_c)(r_c-r), & r\leqslant r_c\\ 0, & r>r_c,\end{cases} \tag{4.2}$$

where $u_{\mathrm{LJ}}(r)$ is given by

$$u_{\mathrm{LJ}}=4\epsilon\left[\left(\frac{\sigma}{r}\right)^{12}-\left(\frac{\sigma}{r}\right)^6\right], \tag{4.3}$$

and $u'_{\mathrm{LJ}}(r_c)=du_{\mathrm{LJ}}(r)/dr|_{r=r_c}$. In the actual simulations $r_c=2.5\sigma$, so that we are dealing with short-range interactions only. Since the shifted-force potential and its first derivative go to zero continuously at $r=r_c$, corrections due to the finite cutoff radius r_c are not required for any of the quantities of interest.

To follow the time evolution of our system, we solve Newton's equation numerically using the so-called velocity Verlet algorithm [37]. To integrate the equation of motion by this finite-difference scheme a time step of $\delta t=4.63\times10^{-3}$ in the customary dimensionless (i.e., ''reduced'') units (see Table I) is used. Energy is then conserved to about 2×10^{-4} for a typical run of 10^5 time steps. Reduced units are also used for all other quantities of interest, which we summarize for convenience in Table I.

Throughout this work we consider $T=1.0$ and a bulk density $\rho_b=0.7$ corresponding to a liquid off any phase coexistence. For this state we determine the chemical potential

TABLE I. Dimensionless (i.e., "reduced") units for various physical quantities; reduced units may be converted to SI units using $m=4.0\times10^{-2}$ kg mol^{-1}, $\sigma=3.4\times10^{-10}$ m, $\epsilon/k_B=120$ K, and $k_B=1.3806\times10^{-23}$ J K^{-1}.

Quantity	In units of
Length	σ
Wave vector	σ^{-1}
Volume	σ^3
Energy	ϵ
Temperature	ϵ/k_BT
Time	$\sqrt{m\sigma^2/\epsilon}$
Velocity	$\sqrt{\epsilon/m}$
Sound attenuation coefficient	$\sqrt{\sigma^2\epsilon/m}$
Thermal diffusivity	$\sqrt{\sigma^2\epsilon/m}$

$\mu=-9.11$ in a canonical ensemble Monte Carlo (CEMC) simulation by means of Widom's test-particle method [37]. In subsequent Monte Carlo simulations in the grand canonical ensemble (GCEMC) we then *fix* $\mu=-9.11$ and determine the *average* fluid density $\rho(s_z)=\langle N\rangle/As_z$ for a range of substrate separations $1.8\leqslant s_z\leqslant 5.0$. For each value of s_z we take $\rho(s_z)$ as input in microcanonical ensemble molecular dynamics (MEMD) simulations. Thus, in MEMD the thermodynamic state of the confined fluid corresponds to $T\approx1.0$ and $\mu\approx-9.11$ (due to slight deviations $\Delta T\simeq\pm1.25\times10^{-2}$ of the mean temperature of the fluid in a given MEMD run from its desired value $T=1.0$) assuming equivalence of statistical-physical ensembles [38].

For each value of s_z and $k_\parallel$, ten MEMD runs were performed. Results presented below were averaged over these runs. Since properties of the confined fluid are translationally invariant in the x and y directions, we chose four equivalent vectors $\boldsymbol{k}_\parallel=(k_x,0)$, $(-k_x,0)$, $(0,k_y)$, and $(0,-k_y)$ corresponding to the same magnitude $k_\parallel$ and average $F(k_\parallel,t)$ over these vectors to further enhance the statistical accuracy of our data. The typical range of $k_\parallel$ covered in this study is $0.075<k_\parallel<0.300$. Note that due to periodic boundary conditions applied at $x=\pm s_x/2$, $y=\pm s_y/2$, k_xs_x and k_ys_y must be integer multiples of 2π. Throughout this work, $s_x=s_y$.

The first of the ten MEMD runs is started from a random configuration of fluid molecules. This configuration is equilibrated in a CEMC simulation using 3×10^4 cycles (i.e., displacement attempts per fluid molecule) [6]. At the end of this equilibration period, velocities are assigned to the fluid molecules. They are taken at random from a Maxwell-Boltzmann distribution for $T=1.0$. This configuration is then equilibrated further in another 10^4 MEMD steps before we begin accumulating data. Runs 2–10 are started from the final configuration of the immediately preceding one.

B. Bulk fluid

We now turn to a discussion of $F(k_\parallel,t)$ for the bulk fluid. Two representative curves for $k_\parallel=0.22$ and 0.38 are plotted in Fig. 1(a). In both cases, $F(k_\parallel,t)$ calculated in MEMD from Eqs. (3.7) and (3.8) is a damped, oscillatory function of time. The larger the period of oscillations, the smaller the $k_\parallel$. Damping, on the other hand, becomes weaker with decreasing $k_\parallel$. Also shown in Fig. 1(a) is a fit of Eq. (3.14) to the MEMD data taking the set $\{D_T,\Gamma,\gamma,v_\parallel\}$ as fit parameters. The plots show that Eq. (3.14) is capable of representing the MEMD-generated data quite nicely over the whole time range plotted and regardless of $k_\parallel$. However, Fig. 1(a) reveals that over the accessible time range, $F(k_\parallel,t)$ does not decay to zero. This effect is more pronounced with decreasing $k_\parallel$, and reflects the increasingly collective nature of propagating density modes as $k_\parallel\to0$.

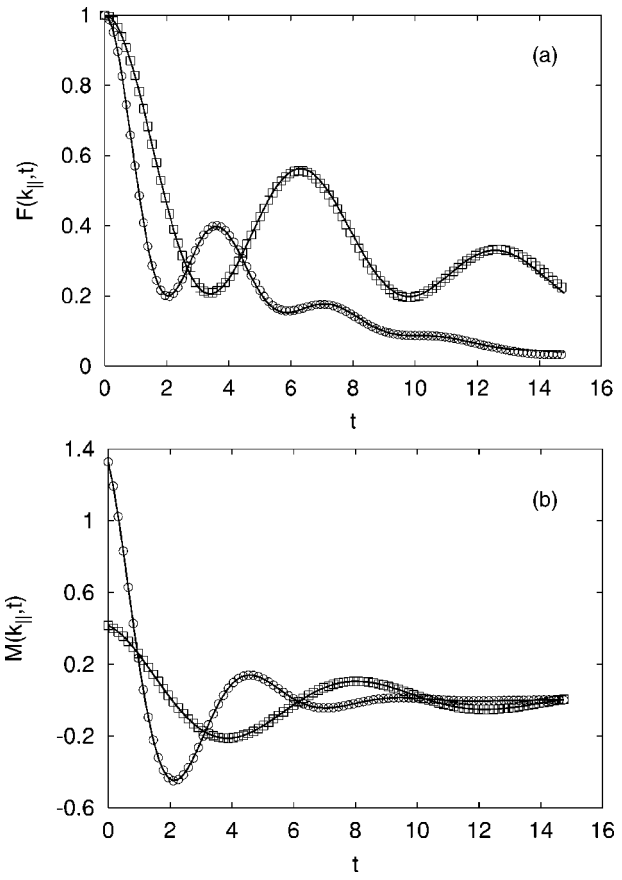

FIG. 1. (a) Intermediate scattering function $F(k_\parallel,t)$ as a function of time t for bulk fluid; (□) $k_\parallel=0.22$, (○) $k_\parallel=0.38$ and solid line is a fit of Eq. (3.14) to MEMD data. (b) is similar to (a), but for $M(k_\parallel,t)$; solid line is fit of Eq. (3.23) ($y''=0$) to discrete data points.

It is also instructive to compare $F(k_\parallel,t)$ with the associated memory function $M(k_\parallel,t)$ plotted in Fig. 1(b). The latter is obtained by solving Eq. (3.15). As pointed out by Berne and Harp [39], rather than solving Eq. (3.15) directly, it is numerically advantageous to first differentiate Eq. (3.15) with respect to t and then solve the resulting expression,

$$M(k_\parallel,t)=-\ddot{F}(k_\parallel,t)-\int_0^t dt'M(k_\parallel,t')\dot{F}(k_\parallel,t-t'),\quad \forall\ k_\parallel, \tag{4.4}$$

in an iterative fashion which requires first and second derivatives of $F(k_\parallel,t)$. These are calculated analytically from Eq.

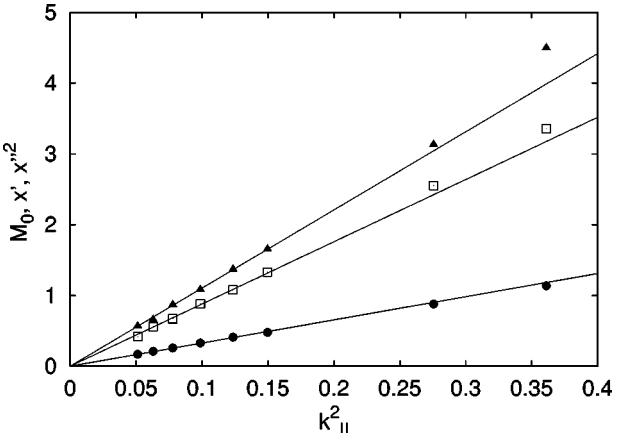

FIG. 2. Scaling laws for $M_0(k_\|)$ (▲), $x'(k_\|)$ (□), and $x''^2(k_\|)$ (●) as functions of $k_\|^2$ obtained by fitting Eq. (3.23) ($y''=0$) to memory function. Straight lines are linear least-squares fits to data points based upon scaling laws [see Eqs. (4.5), (4.7)].

(3.14) using D_T, Γ, γ, and $v_\|$ from the previous fit. Berne and Harp also propose an algorithm by which the so-calculated $M(k_\|,t)$ may be employed to recompute $F(k_\|,t)$ without taking further recourse to an analytic function. These latter data are essentially indistinguishable from the original MEMD-generated $F(k_\|,t)$.

From the plots in Fig. 1(b), we see that $M(k_\|,t)$ oscillates around the t axis in a damped fashion but vanishes more quickly than the corresponding $F(k_\|,t)$ plotted in Fig. 1(a) as one would have expected intuitively from Eq. (3.15). Like $F(k_\|,t)$, the larger $k_\|$ is, the faster $M(k_\|,t)$ goes to zero. However, unlike $F(k_\|,0)$, $M(k_\|,0)\neq 1$, where this initial value reflects the short-time decorrelation of density modes. Therefore, in agreement with Fig. 1(a), $M(k_\|,0)$ increases with $k_\|$. Moreover, it is noteworthy that the hydrodynamic expression given in Eq. (3.23) provides a remarkably good representation of $M(k_\|,t)$ if we take the set $\{x',x'',M_0\}$ as independent fit parameters.

The validity of Eq. (3.23) may be tested further by noting from Eqs. (3.17) and (3.18) that in the hydrodynamic regime ($k_\|\to 0$) the scaling laws

$$x'(k_\|)\propto k_\|^2, \tag{4.5a}$$

$$M_0(k_\|)\propto k_\|^2, \tag{4.5b}$$

must hold because D_T, Γ, γ, and $v_\|$ are independent of $k_\|$. For x'', we have from Eq. (3.17) a slightly more complicated form,

$$x''^2(k_\|)\propto k_\|^2+O(k_\|^4). \tag{4.6}$$

However, we notice from the plots in Fig. 2 that all three quantities can be well represented by straight lines through the origin for $k_\|\lesssim 0.275$. Therefore, we conclude that over this range the contribution of order $k_\|^4$ to x''^2 must be negligible, that is, Eq. (4.6) may be recast as [see also Eq. (3.17)]

$$x''^2\simeq(\gamma-1)M_0(k_\|)\propto k_\|^2. \tag{4.7}$$

From Eq. (3.21), this implies $y''\simeq 0$, so that only the cos term in Eq. (3.23) survives. Let m_1 and m_2 be slopes of linear least-squares fits to the curves $x''^2(k_\|)$ and $M_0(k_\|)$, respectively, where from Eqs. (3.17) and (3.18) one has

$$m_1=\frac{v_\|^2(\gamma-1)}{\gamma}, \tag{4.8a}$$

$$m_2=\frac{v_\|^2}{\gamma}. \tag{4.8b}$$

Combining this last expression with Eq. (4.7), we get

$$\gamma=1+\frac{m_1}{m_2}, \tag{4.9}$$

and therefore from Eq. (4.8b)

$$v_\|=\sqrt{m_1+m_2}. \tag{4.10}$$

Unfortunately, a separate determination of Γ and D_T in the spirit of Eqs. (4.9) and (4.10) is precluded since only x' depends on both quantities [see Eq. (3.17)]. Thus, a fit of Eq. (3.23) in which $\exp(-x't)$ is replaced by $\exp(-\Gamma k_\|^2 t)\exp(-D_T k_\|^2 t/2)$, taking now Γ and D_T as independent parameters, is not able to discriminate between the relative contributions of the two functions. To determine D_T and Γ reliably we notice, however, that, unlike Eq. (3.23), terms depending on Γ and D_T are decoupled in Eq. (3.14) since one of them (Γ) is solely responsible for damping the oscillations whereas the other one (D_T) describes a monotonic decay of $F(k_\|,t)$.

This renders possible the following approach. Based upon the scaling laws stated in Eqs. (4.5) and (4.7) and the slopes of the linear least-squares fits (see Fig. 2), we may calculate x', x'', and M_0 for sufficiently low $k_\|\to 0$. For such a value of $k_\|$, where the required large system sizes renders MEMD simulations unfeasible, we then calculate $M(k_\|,t)$ through Eq. (3.23) ($y''=0$, see above). Inserting this $M(k_\|,t)$ into the Volterra equation [see Eq. (3.15)] and using the algorithm proposed by Berne and Harp [39], we compute a "synthetic" $F(k_\|,t)$ (i.e., one *not* obtained from MEMD) which we analyze through a fit of Eq. (3.14). Applying this procedure for successively lower $k_\|$ enables us to determine the range over which Eq. (3.14) applies, that is, where D_T, Γ, γ, and $v_\|$ are independent of $k_\|$. In Fig. 3 we plot the ratio α_F/α_M, where $\alpha=x'$, x'', M_0, or γ. Subscript F refers to a procedure where we first fit Eq. (3.14) to "synthetic" data points to determine D_T, Γ, $v_\|$, and γ and then use these quantities to calculate x', x'', and M_0 from Eqs. (3.17) and (3.18). If the subscript on α is M we determine x', x'', M_0 from linear least-squares fits to the scaling laws [see Eqs. (4.5) and (4.7) and Fig. 2]; γ is obtained from Eq. (4.9). Since the plots in Fig. 2 show that α_M obeys the scaling laws in Eqs. (4.5) and (4.7) over the entire range of $k_\|$ plotted in Fig. 3, any deviation of α_F/α_M from unity must be ascribed to a failure of Eq. (3.14) that is a dependence of D_T, Γ, $v_\|$, and γ on $k_\|$. Figure 3 shows that such dependences indeed exist for $k_\|>0.1$, say, but that the departure from $k_\|$-independent values

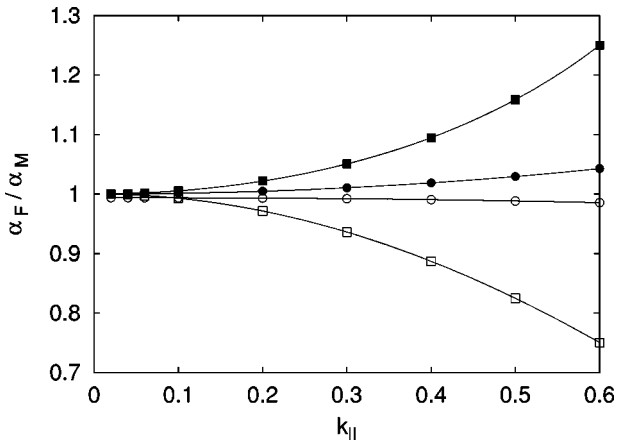

FIG. 3. Ratio α_F/α_M versus $k_\parallel$ for bulk fluid. (■) $\alpha=\gamma$, (●) $\alpha=x''$, (○) $\alpha=x'$, and (□) $\alpha=M_0$, where α is taken from scaling laws [subscript *M*, see Eqs. (4.5), (4.7)] and from "synthetic" $F(k_\parallel,t)$ (subscript *F*, see text).

may be quite different depending on the quantity in question. For example, x' is nearly independent of $k_\parallel$ over the entire range plotted in Fig. 3 whereas a slightly larger and positive deviation is observed for x'' with increasing $k_\parallel$. A much stronger positive and negative deviation is, on the other hand, found for γ and M_0, respectively. As $k_\parallel \to 0$, one expects Eq. (3.14) to become increasingly reliable. This notion is corroborated by the plots in Fig. 3 showing that for $k_\parallel \lesssim 0.1$, $\alpha_F/\alpha_M \simeq 1$. Values for the material constants D_T, Γ, $v_\parallel$, and γ obtained by fitting Eq. (3.14) to "synthetic" data in the range $k_\parallel \lesssim 0.1$ are listed in Table II. Entries in that table show that indeed all four quantities are nearly independent of the particular value of $k_\parallel$ according to one's expectation.

C. Confined fluid

Attending now to a discussion of the confined fluid we begin by plotting in Fig. 4(a) $F(k_\parallel,t)$ from MEMD [see Eqs. (3.7) and (3.8)] for $s_z=1.9$ and 4.1 for the same value of $k_\parallel=0.3142$ together with the corresponding bulk curve. The plots reveal that under confinement the structure of $F(k_\parallel,t)$ is qualitatively the same as for the bulk. Thus, it is not surprising that Eq. (3.14) provides an excellent representation of $F(k_\parallel,t)$ for confined fluids as well. However, one expects from the plots in Fig. 4(a) members of the set $\{D_T,\Gamma,v_\parallel,\gamma\}$ to be affected by the degree of confinement (i.e., the magnitude of s_z, see below).

TABLE II. Material properties D_T, Γ, $v_\parallel$, and γ in the limit $k_\parallel \to 0$. Data were obtained by fitting Eq. (3.14) to "synthetic" $F(k_\parallel,t)$ curves (see text).

$k_\parallel$	D_T	Γ	$v_\parallel$	γ
0.02	1.427	2.537	4.451	2.256
0.03	1.427	2.537	4.451	2.257
0.04	1.427	2.537	4.451	2.257
0.05	1.427	2.537	4.450	2.258
0.06	1.427	2.537	4.450	2.259
0.07	1.427	2.537	4.450	2.260

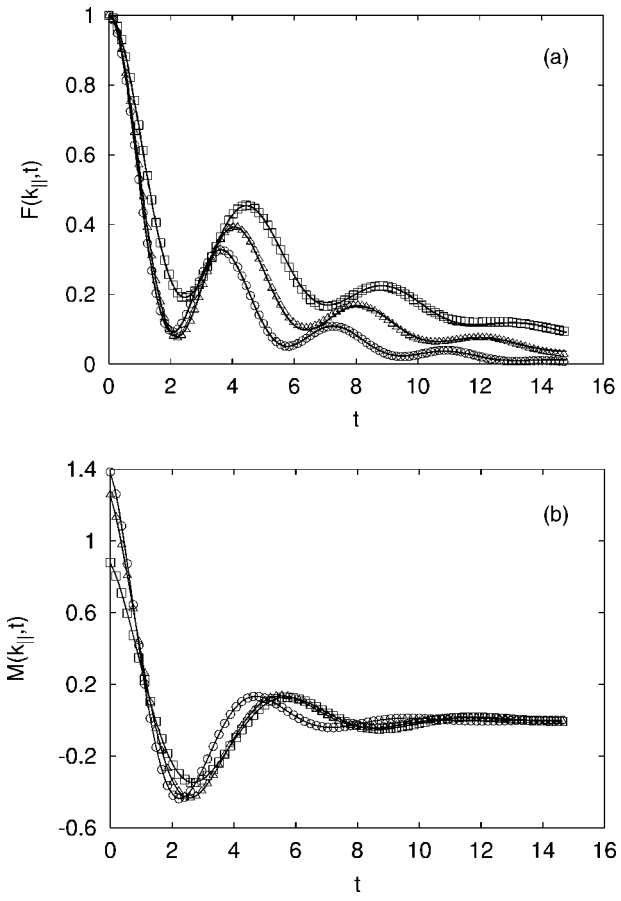

FIG. 4. (a) Intermediate scattering function $F(k_\parallel,t)$ as function of time t for $k_\parallel=0.3142$; (□) bulk fluid, (△) confined fluid, $s_z=4.1$; and (○) confined fluid, $s_z=1.9$. (b) is similar to (a), but for $M(k_\parallel,t)$.

As for the bulk, one may adopt the numerical procedure detailed in Sec. IV B and calculate the corresponding memory function $M(k_\parallel,t)$ by solving Eq. (4.4) in an iterative fashion [39]. Unlike the corresponding plots in Fig. 4(a), $M(k_\parallel,t)$ is somewhat less sensitive to s_z. This is particularly obvious if one compares the curves in Figs. 4 corresponding to $s_z=1.9$ and 4.1 with their bulk counterpart.

In order to determine $D_T(s_z)$, $\Gamma(s_z)$, $v_\parallel(s_z)$, and $\gamma(s_z)$, we intend to apply the procedure described in Sec. IV B. As shown in that section the analysis rests upon the scaling laws for the parameters x', x'', and M_0 of the memory function [see Eqs. (4.5) and (4.7)]. Thus, it seems sensible to plot in Fig. 5, x' versus $k_\parallel$ for $s_z=1.9$ and 4.1 in comparison with the corresponding bulk curve. As one can see from the plot the scaling law [see Eq. (4.5a)] is obeyed by the confined fluid as well. We have checked that this holds also for x'' [see Eq. (4.7)] and M_0 [see Eq. (4.5b)]. Thus, we may adopt the procedure applied to the bulk and determine $D_T(s_z)$, $\Gamma(s_z)$, $v_\parallel(s_z)$, and $\gamma(s_z)$ through a fit of Eq. (3.14) to synthetic data for $F(k_\parallel,t)$ for $k_\parallel \lesssim 0.1$.

Results are plotted in Fig. 6 for $\alpha_{\text{slit}}/\alpha_{\text{bulk}}$, where $\alpha = D_T$, b (see Sec. II B) or $v_\parallel$, that is, we normalize each quantity to the bulk value listed in Table II. The plots show that D_T, b, and $v_\parallel$ oscillate with a period of about one mo-

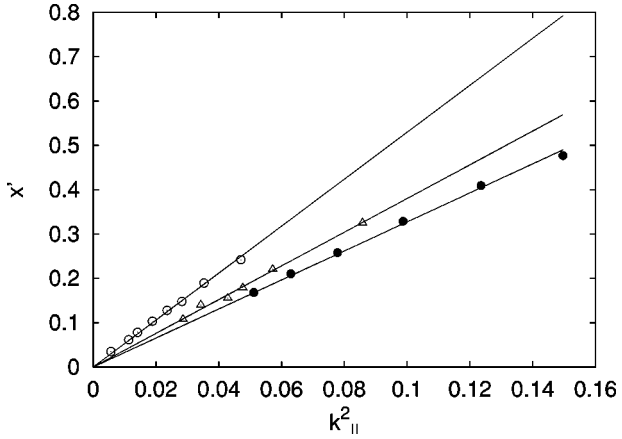

FIG. 5. Scaling law for x' as function of $k_{\|}^2$; (○) confined fluid, $s_z=1.9$, (△) confined fluid, $s_z=4.1$, and (●) bulk.

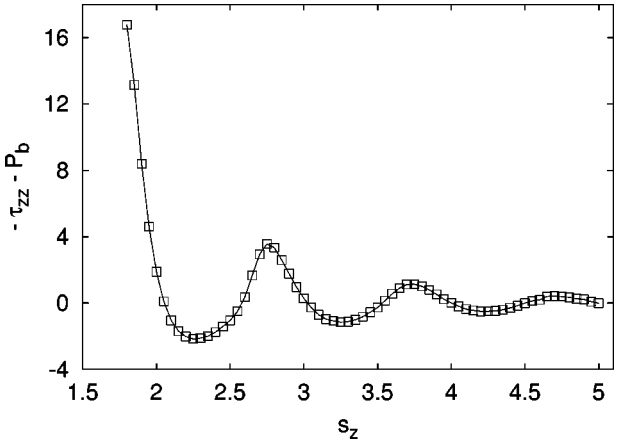

FIG. 7. Solvation pressure $-\tau_{zz}-P_b$ as function of substrate separation s_z. Data were obtained in GCEMC for $T=1.0$, $\mu=-9.11$. Solid line is fit to data point intended to guide the eye.

lecular "diameter" as s_z increases. The oscillations are damped so that $\{D_T,b,v_{\|}\}$ assume their (s_z-independent) bulk values for $s_z \gtrsim 20$ to within 3% as we have checked. Maxima and minima are detected at about the same value of s_z. The magnitude of the confinement effect decreases in the order $D_T \rightarrow b \rightarrow v_{\|}$.

The rather similar periodic structure of the plots in Fig. 6 prompted us to attempt to correlate them with variations in the so-called solvation pressure $-\tau_{zz}-P_b$ (τ_{zz} is the component of the stress tensor and P_b is the bulk pressure) of a confined fluid in thermodynamic equilibrium with the bulk which may be calculated as a function of s_z in GCEMC simulations for fixed T and μ [see Eqs. (93)–(96) in Ref. [29]]. In the infinite-system limit, that is for $s_z \rightarrow \infty, \tau_{zz} \rightarrow -P_b$ according to the definition of τ_{zz} [29]. As shown in Fig. 7, $-\tau_{zz}-P_b$ oscillates around the ordinate as expected.

A correlation between $-\tau_{zz}$ and structural changes in the confined fluid is established most directly by comparison with the local density $\rho(z)$. From such an analysis it is apparent that for "simple" fluids the oscillatory dependence of τ_{zz} on s_z reflects stratification (i.e., the arrangement of (spherical) fluid molecules in individual layers parallel with the confining substrates, see Sec. IV A 2 of Ref. [29] and additional references therein). Oscillations in $-\tau_{zz}$ are therefore fingerprints of the formation of a full new layer of fluid molecules. Consequently these maxima are separated roughly by one molecular diameter similar to the extrema of D_T, b, and $v_{\|}$ (see Fig. 6). At minima of $-\tau_{zz}$, the fluid is under minimum compressional stress and hence fluid molecules are most conveniently accommodated between the substrates (i.e., the fluid is more ordered). At maxima of $-\tau_{zz}$, on the other hand, the layered fluid structure is disrupted maximally (i.e., the fluid is most disordered). Comparing the plots in Figs. 6 and 7 one realizes that in the more ordered states sound waves propagate with a higher velocity but appear to be damped more strongly in comparison with more disordered states. Finally, we present plots of $S(k_{\|},\omega)$ in Fig. 8, which we calculate from

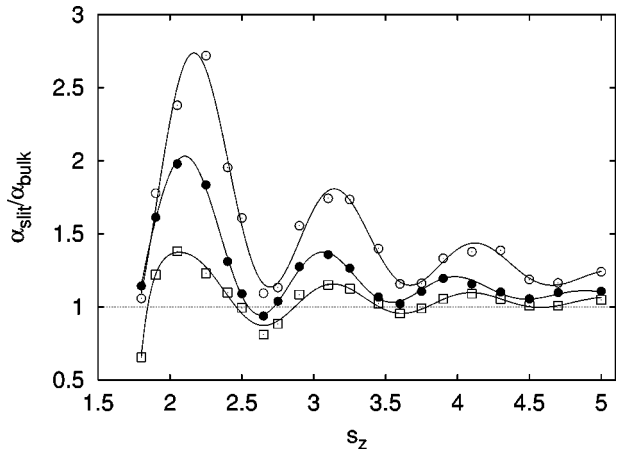

FIG. 6. Ratio $\alpha_{\text{slit}}/\alpha_{\text{bulk}}$ versus s_z for thermal diffusivity D_T (○), lateral kinematic viscosity b (●), and adiabatic, in-plane velocity of sound $v_{\|}$ (□).

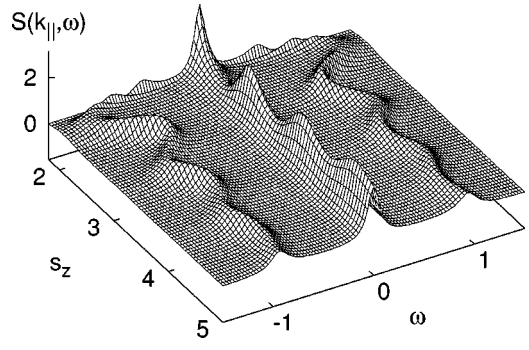

FIG. 8. Dynamic structure factor $S(k_{\|},\omega)$ as a function of ω and for various substrate separations s_z and $k_{\|}=0.20$. Results are obtained using interpolated data for D_T, b, $v_{\|}$, and γ from Fig. 6 in Eq. (4.11).

$$S(k_\parallel,\omega)=\mathrm{Re}\,F(k_\parallel,\omega)$$
$$=\frac{\gamma}{\gamma-1}\frac{D_T k_\parallel^2}{\omega^2+(D_T k_\parallel^2)^2}+\frac{1}{2\gamma}\left[\frac{\Gamma k_\parallel^2}{(\omega-v_\parallel k_\parallel)^2+(\Gamma k_\parallel^2)^2}-\frac{d(k_\parallel)(\omega-v_\parallel k_\parallel)}{(\omega-v_\parallel k_\parallel)^2+(\Gamma k_\parallel^2)^2}\right]$$
$$+\frac{1}{2\gamma}\left[\frac{\Gamma k_\parallel^2}{(\omega+v_\parallel k_\parallel)^2+(\Gamma k_\parallel^2)^2}+\frac{d(k_\parallel)(\omega+v_\parallel k_\parallel)}{(\omega+v_\parallel k_\parallel)^2+(\Gamma k_\parallel^2)^2}\right], \tag{4.11}$$

which follows from Eq. (3.13) by replacing s by $i\omega$. To obtain Fig. 8 we chose $k_\parallel=0.20$ so that the results pertain roughly to the light scattering in the vacuum ultraviolet regime. For such a small value of $k_\parallel$ one expects $d(k_\parallel)\approx 0$ and Eq. (4.11) reduces to a sum of three Lorentzians, one centered at $\omega=0$ (Rayleigh line) and the other two at $\omega=\pm v_\parallel$ (Brillouin lines). As a consequence of the oscillatory dependence of D_T on s_z, the height of the Rayleigh peak oscillates with a period of about σ as s_z increases. On account of the oscillatory dependence of $v_\parallel$ on s_z a periodic shift of the two Brillouin peaks along the ω axis is also observed in Fig. 8. Following McIntyre and Sengers, the first term on the far right side of Eq. (4.11) can be identified with the (nonpropagating) decay of entropy fluctuations such that for $\omega=0$ the height of the Rayleigh peak is a measure of the entropy of the fluid (divided by $D_T k_\parallel^2$) [35]. In view of this, it is not surprising that $S(k_\parallel,0;s_z)$ oscillates with s_z (see Fig. 8) such that the maxima correspond to the states of maximum disorder of the confined fluid identified through a parallel analysis of the solvation pressure (see above). The Brillouin peaks, on the other hand, describe propagating transverse-pressure modes at constant entropy [35].

V. SUMMARY AND CONCLUSIONS

In this work we are concerned with the propagation of density modes in a fluid confined to nanoscopic spaces by unstructured (i.e., laterally smooth) solid substrates. Our focus is on the hydrodynamic regime for which we develop relevant conservation laws in Sec. II A. The key in deriving these expressions is coarse graining the fluid's structural and temporal properties. This is achieved by introducing a volume element V that is both small on a macroscopic but large on a molecular scale. Hydrodynamics is then concerned with fluxes in and out of V through its surface. Assuming V to be of arbitrary shape and extent in the x-y plane but to cover the entire space between the substrate surfaces in the z direction, we derive conservation laws for z-averaged lateral fluxes (i.e., fluxes in directions parallel with the substrate surfaces). This approach seems sensible since the fluid is *on average* homogeneous and isotropic in the x-y plane on account of the fluid substrate potential that is solely a function of the distance in the z direction between a fluid molecule and both substrates [see Eq. (4.1)]. Because of this lateral homogeneity and isotropy, we assume constitutive equations for momentum and energy fluxes identical with those commonly employed for bulk fluids. With these constitutive equations we derive a set of coupled linear equations that can be solved for propagating density modes in the hydrodynamic regime. Using this last expression together with the microscopic definition of the intermediate scattering function eventually leads to an expression for $F(k_\parallel,t)$ in the hydrodynamic regime.

However, to obtain $F(k_\parallel,t)$ from the more directly accessible $F(k_\parallel,s)$, the latter needs to be Laplace inverted. This inversion is only *approximately* possible because of the complexity of the hydrodynamic $F(k_\parallel,s)$ [see Eq. (3.10)]. As a result the *form* of $F(k_\parallel,t)$ is correct only to order $O(k_\parallel^2)$. However, if the hydrodynamic $F(k_\parallel,t)$ is fitted to MEMD data for the accessible range of $k_\parallel$, the fit parameters (i.e., the set $\{D_T,\Gamma,v_\parallel,\gamma\}$) turn out to depend on $k_\parallel$. This reflects a deficiency of the hydrodynamic $F(k_\parallel,t)$ caused by the crudeness of the assumptions [see Eqs. (3.11) and (3.12)] invoked to derive Eq. (3.14) from Eq. (3.10).

We therefore propose a different approach in this work by which propagating hydrodynamic modes can be analyzed and interpreted more reliably. Rather than employing directly $F(k_\parallel,t)$, its memory function $M(k_\parallel,t)$ turns out to be more useful. The two are related through the Volterra integrodifferential equation. In the hydrodynamic regime this equation can be solved *exactly* for $M(k_\parallel,s)$ using the hydrodynamic form of $F(k_\parallel,s)$ [see Eq. (3.10)]. The advantage of $M(k_\parallel,t)$ over $F(k_\parallel,t)$ is that its limiting hydrodynamic form is not based upon any additional assumptions than those necessary to derive Eqs. (2.22)–(2.24). Because of its relative simplicity, $M(k_\parallel,s)$ can be transformed back to the time domain analytically and expressed in terms of x', x'', M_0, and γ [see Eqs. (3.17), (3.18), (3.21), and (3.23)].

Members of the set $\{x',x'',M_0,\gamma\}$ obey simple analytic scaling laws [see Eqs. (4.5) and (4.7)] that may be employed to calculate $F(k_\parallel,t)$ from $M(k_\parallel,t)$ by solving numerically Eq. (3.15) for $k_\parallel\lesssim 0.1$ where a direct calculation from MEMD is unfeasible on account of the large system sizes that would be required. However, by fitting the hydrodynamic expression for $F(k_\parallel,t)$ [see Eq. (3.14)] to these synthetic data, $k_\parallel$-independent results for $\{D_T,\Gamma,v_\parallel,\gamma\}$ are eventually obtained. The regime of $k_\parallel$, where the form of $F(k_\parallel,t)$ becomes approximately correct, is about a factor of 2 smaller than *assumed* previously in the work of Schoen *et al.* for homogeneous bulk fluids [27]. The interpolation of $\{D_T,\Gamma,v_\parallel,\gamma\}$ towards $k_\parallel=0$ (i.e., the infinite-system limit) carried out by these authors must be regarded as unsafe and the apparent agreement with experimental results is fortuitous in the light of the present study.

The analysis of both $M(k_\parallel,t)$ and $F(k_\parallel,t)$ can be carried out for confined fluids as well. Results for the set $\{D_T,b,v_\parallel\}$ reveal a confinement effect manifested as an oscillatory dependence of all three members of the set on the substrate separation s_z (see Fig. 6). Correlating the oscillations in $\{D_T,b,v_\parallel\}$ with similar oscillations in the solvation pressure, which are well understood for ''simple'' fluids, permits us to conclude that for values of s_z where an integer number of

fluid layers fits best between the solid substrates (i.e., states of a high degree of order) are characterized by maxima of $\{D_T, b, v_\parallel\}$, whereas in situations where the formation of a new layer is in progress, the three quantities become minimum.

In the near future we intend to employ the approach developed here to investigate the dynamics of confined fluids near first-order phase transitions. If, for example, the thermodynamic state of the fluid approaches its limit of stability (i.e., a spinodal) from either the liquid or gas one-phase region, one expects the isothermal compressibility $\kappa_\parallel$ to become large (see Sec. III C). Because of Eq. (2.25a), this implies $v_\parallel \to 0$. It might therefore be conceivable that for a given thermodynamic state in the vicinity of a phase transition, $x'' \to 0$ in Eq. (3.17). Hence, $\cosh(ix''t)$ and $\sinh(ix''t)$ in Eq. (3.20) may be replaced by 1 and 0, respectively. One therefore expects a significant change of $M(k_\parallel, t)$ from a damped oscillatory function of t to a simple exponential, that is,

$$M(k_\parallel, t) = M_0(k_\parallel)\exp(-x't). \tag{5.1}$$

If, on the other hand, $v_\parallel$ becomes sufficiently small, the inequality in Eq. (3.22) may have to be replaced by

$$M_0(k_\parallel) < \frac{(D_T k_\parallel^2 \gamma - x')^2}{\gamma - 1}, \tag{5.2}$$

so that x'' becomes complex and hence $M(k_\parallel, t) = \mathrm{Re}\, M(k_\parallel, t) + \mathrm{Im}\, M(k_\parallel, t)$ [see Eq. (3.20)], where the real part

$$\mathrm{Re}\, M(k_\parallel, t) = \frac{M_0(k_\parallel)}{2}\{\exp[-(x' + x'')t] + \exp[-(x' - x'')t]\}. \tag{5.3}$$

However, one has to keep in mind that the present theory is based upon linearized hydrodynamic equations like Eqs. (2.16) and (2.19). Since fluctuations become large as one approaches the limit of stability of a fluid, the validity of the present approach in the context of phase equilibria remains to be tested. This test is possible on the basis of parallel GCEMC simulations where the location of first-order phase transitions can be located precisely through a calculation of the grand potential [40].

ACKNOWLEDGMENTS

We thank Dr. S. H. L. Klapp and Professor D. J. Diestler (University of Nebraska–Lincoln) for many helpful discussions and a critical reading of the original manuscript. Moreover, we are grateful for support from the Sonderforschungsbereich 448 ''Mesoskopisch Strukturierte Verbundsysteme.''

[1] H. Bock, D.J. Diestler, and M. Schoen, J. Phys.: Condens. Matter **13**, 4697 (2001).
[2] M. Schoen, J.H. Cushman, and D.J. Diestler, Mol. Phys. **81**, 475 (1994).
[3] L.D. Gelb, K.E. Gubbins, R. Radhakrishnan, and M. Sliwinska-Bartkowiak, Rep. Prog. Phys. **62**, 1573 (1999).
[4] L. A. Pozhar, *Transport Theory of Inhomogeneous Fluids* (World Scientific, Singapore, 1994).
[5] D. N. Theodorou, R. Q. Snurr, and A. T. Bell, in *Comprehensive Supramolecular Chemistry*, edited by G. Alberti and T. Bein (Elsevier Science, Oxford, 1996), Vol. 7.
[6] M. Schoen, D.J. Diestler, J.H. Cushman, and C.L. Rhykerd, Jr., J. Chem. Phys. **88**, 1394 (1988).
[7] J. Kärger and D. M. Ruthven, *Diffusion in Zeolites and Other Microporous Materials* (Wiley, New York, 1992).
[8] R. Haberlandt and J. Kärger, Chem. Eng. J. **74**, 15 (1999).
[9] M. Gaub, S. Fritzsche, R. Haberlandt, and D.N. Theodorou, J. Phys. Chem. B **103**, 4721 (1999).
[10] D.T. On, D. Desplantier-Giscard, C. Danumah, and S. Kaliaguine, Appl. Catal. A **222**, 299 (2001).
[11] N. Y. Chen, T. F. Degan, Jr., and C. M. Smith, *Molecular Transport and Reaction in Zeolites: Design and Application of Shape Selective Catalysts* (Wiley-VCH, New York, 1994).
[12] K.P. Travis and K.E. Gubbins, Langmuir **15**, 6050 (1999).
[13] N.A. Seaton, S.P. Friedman, J.M.D. MacElroy, and B.J. Murphy, Langmuir **13**, 1199 (1997).
[14] J.M.D. MacElroy and M.J. Boyle, Chem. Eng. J. **74**, 85 (1999).
[15] I. Bitsanis, T.K. Vanderlick, M. Tirrell, and H.T. Davis, J. Chem. Phys. **89**, 3152 (1988).
[16] K.P. Travis, B.D. Todd, and D.J. Evans, Phys. Rev. E **55**, 4288 (1997).
[17] K.P. Travis and K.E. Gubbins, J. Chem. Phys. **112**, 1984 (2000).
[18] L. Pozhar, Phys. Rev. E **61**, 1432 (2000).
[19] V.P. Sokhan, D. Nicholson, and N. Quirke, J. Chem. Phys. **115**, 3878 (2001).
[20] J. Klein and E. Kumacheva, J. Chem. Phys. **108**, 6996 (1998).
[21] E. Kumacheva and J. Klein, J. Chem. Phys. **108**, 7010 (1998).
[22] W. Brown, *Dynamic Light Scattering* (Clarendon, Oxford, 1993).
[23] B. J. Berne and R. Pecora, *Dynamic Light Scattering* (Wiley, New York, 1976).
[24] C.H. de Novion, Radiat. Phys. Chem. **51**, 637 (1998).
[25] J. B. Hayter, in *Neutron Spin Echo*, edited by F. Mezei (Springer-Verlag, Berlin, 1980), p. 53.
[26] F. Mezei, in *Neutron Spin Echo*, edited by F. Mezei (Springer-Verlag, Berlin, 1980), p. 3.
[27] M. Schoen, R. Vogelsang, and C. Hoheisel, Mol. Phys. **57**, 445 (1986).
[28] J. P. Boon and S. Yip, *Molecular Hydrodynamics* (McGraw-Hill, New York, 1980), Chap. 5.3.
[29] M. Schoen, in *Computational Methods in Surface and Colloid Science*, edited by M. Borówko (Dekker, New York, 2000), Chap. 1.
[30] L. D. Landau and E. M. Lifshitz, *Fluid Mechanics*, Course of

Theoretical Physics Vol. 6 (Pergamon, Oxford, 1963), p. 49.
[31] J. P. Hansen and I. R. McDonald, *Theory of Simple Liquids*, 2nd ed. (Academic, London, 1986).
[32] M. Schoen, Physica A **270**, 353 (1999).
[33] L. van Hove, Phys. Rev. **95**, 249 (1954).
[34] R.D. Mountain, Rev. Mod. Phys. **38**, 205 (1966).
[35] D. McIntyre and J. V. Sengers, in *Physics of Simple Liquids*, edited by H. N. V. Temperley, J. S. Rowlinson, and G. S. Rushbrooke (North Holland, Amsterdam, 1968), p. 480.
[36] B. J. Berne, in *Physical Chemistry. An Advanced Treatise*, edited by H. Eyring, D. Henderson, and W. Jost (Academic, London, 1971), Vol. VIIIB.
[37] M. P. Allen and D. J. Tildesley, *Computer Simulation of Liquids* (Academic, London, 1987), Chap. 3.2.1.
[38] T. L. Hill, *Statistical Mechanics, Principles and Selected Applications* (Dover, Mineola, NY, 1987), Chap. 20.
[39] B.J. Berne and G.D. Harp, Adv. Chem. Phys. **17**, 63 (1970).
[40] M. Schoen, Colloids Surf. A: Physicochem. Eng. Asp. **206**, 253 (2002).